International Symposium
On Turbulence and Shear Flow
Phenomena (TSFP-9)
June 30 - July 3, 2015 *Melbourne, Australia*

EFFECTS OF SUDDEN CHANGE IN SURFACE ROUGHNESS ON TURBULENT BOUNDARY LAYERS

Ronald E. Hanson
Aerodynamics and Flight Mechanics Research Group
University of Southampton
Southampton, SO17 1BJ, UK
R.E.Hanson@soton.ac.uk

Bharathram Ganapathisubramani
Aerodynamics and Flight Mechanics Research Group
University of Southampton
Southampton, SO17 1BJ, UK
G.Bharath@soton.ac.uk

ABSTRACT

In this experimental study the response of the turbulent boundary layer to a sudden change in surface condition, from rough to smooth wall, is examined. The flow field is interrogated by hot-wire anemometry and particle imaging velocimetry while the local skin friction is determined by Preston tube measurements. An internal boundary layer represents the demarkation between the characteristic flow of the upstream rough wall condition and the region developing over the smooth surface. Two distinct energetic regions within the boundary layer are observed downstream of the roughness. Within the internal layer the flow over the smooth surface and the corresponding near-wall turbulence establishes under the influence of the outer region that persists from the incoming rough-wall. Energy contained in the outer region diminishes downstream and the behaviour of the near-wall begins to resemble that of a smooth wall boundary layer in equilibrium. Above the internal layer the structure of the outer region appears to be independent of the near-wall condition, however, the structure of the near-wall region depends on the local near wall condition.

INTRODUCTION

The turbulent boundary layer occurring over a surface which transitions abruptly from a rough-to-smooth (R→S) boundary condition results in a non-equilibrium condition. As discussed by Jiménez (2004), roughness appears to be a more efficient generator of skin friction than smooth walls. Immediately after the R→S interface the local skin friction is reduced well below both the rough-wall value, as well as the comparable smooth wall value, see for example Antonia & Luxton (1972) and Taylor *et al.* (1993), but then increases toward the equilibrium smooth wall value downstream. In fact, the near wall peak in the streamwise stress appears to develop immediately following the R→S interface (Antonia & Luxton, 1972; Taylor *et al.*, 1993). This scenario suggests that the entire boundary layer does not immediately adapt to the new surface condition. Rather, following the surface change a single internal layer develops that represents a demarkation of the boundary layer characteristics. Above this layer the flow is characteristic of the upstream condition. Within the internal layer the near-wall turbulence establishes itself under the influence of the outer region that remains from the incoming rough-wall. Therefore two distinct energetic regions within the boundary layer are observed downstream of the roughness. Further review and detailed significance of perturbed flows are found in Smits & Wood (1985).

In this experimental study the response of the boundary layer that transitions from a rough to smooth surface is considered. The objective of this study is to examine the interaction between the outer region that persists from upstream conditions and the newly established near-wall region. The flow field is interrogated by hot-wire anemometry and particle imaging velocimetry while the local skin friction is determined by Preston tube measurements. We examine the scaling of the resulting non-equilibrium boundary layer from the perspective of outer variable scaling and also from the perspective of inner variable scaling. The current study extends the mean flow and statistical analysis of Antonia & Luxton (1972) to an understanding of how these previous observations manifest energetically by examining the turbulence spectra across the boundary layer. Furthermore, the structure and evolution of the turbulence is examined to offer insight into potential physical mechanisms that may occur.

EXPERIMENTAL DETAIL

Experiments were performed in a suction-type wind tunnel at the University of Southampton. The tunnel has a 7:1 contraction followed by a 4.5 m long working section having a 0.9 m $\times$ 0.6 m cross section, diffuser and fan. A turbulent boundary layer was established on a 10 mm thick boundary layer plate mounted in the test section. The leading edge of the plate is machined from aluminium to a 15 degree angle, such that the measurement side of the plate is flat over the entire length. For the rough-to-smooth surface change, the first 2.3 m downstream of the leading edge

was fitted with a rough surface followed by an additional 1.8 m fetch of smooth wall. The rough surface considered in this study is a16-gauge industrial open-type silicone carbide abrasive sheet, which can be considered a sparse, isotropic, and highly non-Gaussian surface, as shown and used in Birch & Morrison (2011). The maximum roughness height (k_{max}) is approximately 2 mm.

Single and two-component hot-wire measurements were performed simultaneously; the two-component measurements were made to infer the shear stress occurring over the rough surface. The mean and fluctuating velocities along the streamwise and wall-normal (x,y) directions are represented by (U,V) and (u,v). The Auspex A55P05 boundary layer probe had a 5 μm diameter tungsten wire with a central 1.05 mm active region, such that the resulting length to diameter ratio is 210. The two-component probe was a Dantec model 55P61 hot-wire. Each hot-wire was operated by constant temperature anemometers (CTAs) with an overheat ratio of 1.8. For the single wire a modified version of King's Law was fit to calibration data, where the exponent is included in the fitted parameters. For the cross-wire a look-up-table calibration was used to reduce the data into u and v velocity components as described by Burattini & Antonia (2005). The hot-wires were calibrated statically in the test section of the wind tunnel against a Pitot-static tube connected to a Furness FCO510 0 - 200 Pa pressure transducer over a range of velocities between 1.2 m/s and $1.2U_\infty$, where U_∞ is the freestream velocity of the experiments, 10 m/s. The temperature was monitored throughout the experiments to correct the CTA output signals to the reference calibration temperature (see Bruun, 1995), although the ambient temperature remained within $\pm$0.7 degrees Celsius. The wall-normal position of the hot-wires was controlled by a Parker Automation linear traverse in conjunction with a PDX series ministep drive. At each measurement location a sample length, T, between 16000 and 20000 boundary-layer turnover times (TU_∞/δ), where δ is the boundary layer thickness, was used to converge the energy contained in the largest scales following the recommendation of Hutchins *et al.* (2009). The total uncertainty of the mean velocity measurements is within $\pm$1.1%.

Over the smooth wall the surface shear stress was estimated using the Preston tube method, which has been utilized for wall shear stress measurements following a R$\rightarrow$S change in surface condition (Antonia & Luxton, 1972; Loureiro *et al.*, 2010, for example). In the recent study by Loureiro *et al.* (2010) several methods to determine the wall shear were compared. The Preston tube method was shown to agree within 10% of the shear stress determined from the near-wall profile, whereas Taylor *et al.* (1993) suggests an accuracy within 6%. Note that Loureiro *et al.* (2010) only considered regions where $x/\delta < 1.5$ where the uncertainly of Preston tube measurements are highest, as discussed by Antonia & Luxton (1972). Therefore, the measurements of the fiction velocity are considered reliable and useful, except very near the R$\rightarrow$S surface change.

Wide-field Particle Image Velocimetry (PIV) measurements were made using images recorded at resolution of 3248$\times$4872 pixels from two side-by-side ImagerProLX CCD cameras with 200mm Nicon macro lens. The flow was seeded with a particles produced by vaporizing a glycol-water solution using a Jem ZR12-DMX fog generator. The streamwise/wall-normal plane was illuminated by a double-pulsed Nd:YAG Litron Laser (200 mJ/pulse). Velocity fields were processed with PIV software from LaVision, using a multi-pass approach, with windows of 64^2 and then down to 16^2 pixels at 50% overlap to produce each velocity vector. The resulting resolution per processed vector is 0.25 mm^2, and data were averaged over 5000 vector fields. Two measurement regions of the flow were captured by repositioning the dual camera setup. The first was from approximately x = -52 to 253 mm, and the second from x = 480 to 785 mm. The wall-normal region captured extends from approximately 0.6 mm to 102 mm, although over the region of the roughness the field of view was limited by the roughness height.

RESULTS

Following an abrupt change in the wall surface from R$\rightarrow$S the properties of the boundary layer vary from first reflecting those of a rough wall to a fully smooth wall downstream and are known to vary rather slowly (Antonia & Luxton, 1972). The variation of the shape factor, $H_{12} = \delta^*/\theta$, where δ^* and θ are the displacement and momentum thicknesses, respectively, are shown in figure 1 and includes the development of the boundary layer thickness. The shape factor decreases over the smooth wall from the upstream rough wall condition. At the final measurement station, $x = 1.32$ m, $H_{12} \approx 1.38$. The corresponding Reynolds number, $\mathrm{Re}_\theta = \theta U_\infty/\nu \approx 6400$, at this location would exhibit $H_{12} \approx 1.36$ for a self-preserving smooth wall boundary layers following from the formulation of Nagib *et al.* (2007).

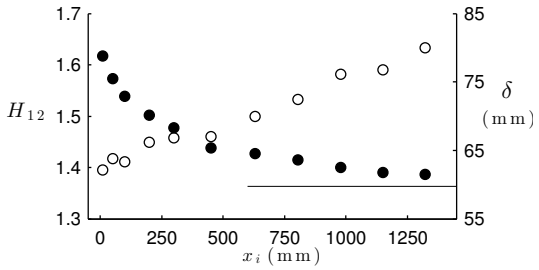

Figure 1. Shape factor development downstream of the rough-smooth interface, •, and corresponding growth of the boundary layer thickness, ○.

The strength of the roughness step, $M_{R\rightarrow S}$, is normally expressed as the logarithmic difference between two roughness heights $\ln(y_{01}/y_{02})$, where y_{01}/y_{02} is the ratio of the roughness lengths for the oncoming and downstream flow relative to the rough-to-smooth change in the surface condition. For further detail see, for example, Andreopoulos & Wood (1982). In the present results, y_{01} was determined at approximately 5δ upstream of the R$\rightarrow$S surface change, and y_{02} was measured at the final downstream station where the shape factor is near that of a self-preserving smooth-wall boundary layer. For a smooth wall, both d and $\Delta U/U_\tau$ are zero, which was the case in the calculation of y_{02}. The resulting strength of the roughness step is $M_{R\rightarrow S} = 2.1$.

Following an abrupt R$\rightarrow$S change the skin friction immediately decreases and begins to recover to that of a comparable smooth wall boundary layer (Antonia & Luxton, 1972, for example). Over the rough surface the friction velocity, U_τ, is estimated from the Reynolds stress plateau using the cross-wire measurements (see for example Flack *et al.*, 2005). The skin friction coefficient, c_f, is

related to the friction velocity by $c_f = \tau_w/0.5\rho U_\infty^2$, where $U_\tau = (\tau_w/\rho)^{1/2}$. Prior to the R→S change $c_f \approx 38 \times 10^{-4}$. Along the smooth surface the friction velocity was estimated by the Preston tube method. The resulting variation of c_f is shown in figure 2. For comparison the both Preston tube measurements and values inferred from a semi-log plot of the mean velocity are included. Excellent agreement between these measurements is shown, within 4% for $x/\delta > 0.8$. The discrepancy is highest near the R→S surface change where the value determined from a semi-log plot is approximately 40% higher than the corresponding Preston tube measurement at $x/\delta = 0.16$. An additional dataset is included from Antonia & Luxton (1972) for comparison, although the step strength is not formally reported by the authors, regardless, the trends appear similar.

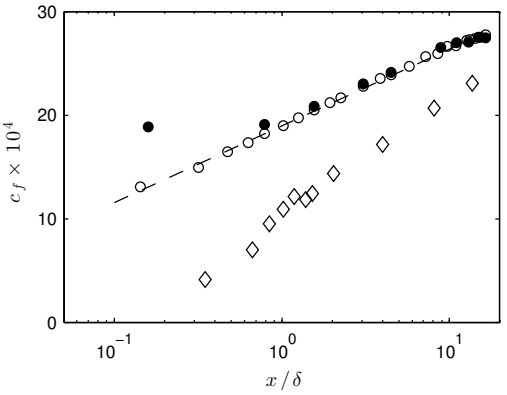

Figure 2. Variation of the skin fiction coefficient, c_f, with x/δ using the Preston tube method, ◦, and inferred from semi-log plots of mean velocity, •. Data is fit by $c_f = f(M)\log(x/\delta) + g$, − − −. Additional data from Antonia & Luxton (1972) is given by ⋄.

Normalizing the streamwise coordinate with the local boundary layer thickness, δ, produces a trend in the skin friction coefficient that can be represented by the relationship, $c_f = f(M_{R\to S})\log(x/\delta) + g$, and is included in figure 2. The form of this equation shows that the strength of the step affects the slope of the resulting c_f curve in semi-log form. This suggests that the step strength of the included data of Antonia & Luxton (1972) occurs at a larger value of $M_{R\to S}$. Although, the physical meaning of the offset (g) is less clear, it is however possible to speculate on its form. In one instance it should be related to the roughness scale of the incoming flow, y_{01}, however, this value should be also depend on the Reynolds number owing to the established relationship between c_f and Re_θ as shown by Österlund *et al.* (2000).

A selection of the mean streamwise velocity profiles are plotted in semi-logarithmic format in figure 3 in terms of the traditional outer variables, U_∞ and δ. Downstream of the surface roughness change a significant velocity deficit occurs, which is particularly evident at $y/\delta < 0.3$. This height corresponds to approximately 10 times the maximum roughness height and this deficit appears to persists to the furtherest downstream measurement location.

From the skin friction coefficient shown in figure 2 it is possible to consider the boundary layer in terms of the inner scaling ($y^+ = yU_\tau/\nu$ and $U^+ = U/U_\tau$) as shown in figure

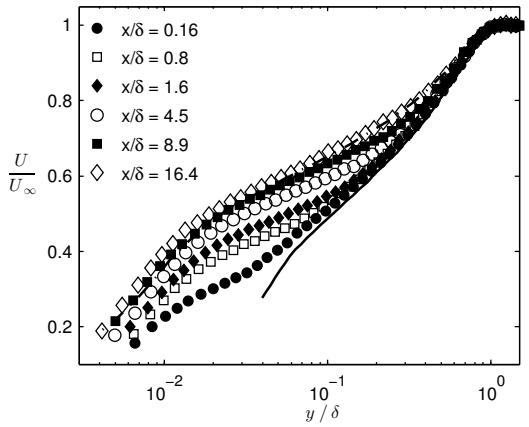

Figure 3. Outer scaling of selected mean streamwise velocity profiles. The upstream rough wall profiles is shown by —— and the symbols indicate the profiles above the smooth surface.

4. Profiles obtained past the first measurement station at $x =$ 10 mm collapses well in the near-wall region for $y^+ < 30$. Compared to the law of the wall for smooth-walls, the well-known characteristic of the rough surface is the shifting the logarithmic portion of wall curve as is shown in figure 4 where the abscissa is represented by $(y-d)^+$ for the rough wall case. Antonia & Luxton (1972) notes that near the R→S transition there is reason to doubt the reliability of the Preston tube measurements, which rely on the logarithmic law, and therefore the large deviation observed for the first position may be an artifact of this uncertainty. Regardless, the collapse of the near-wall region is remarkable. The most salient feature of figure 4 is the deviation of U^+ for $y^+ >$ 200. The downstream profiles collapse toward the smooth wall case, although the Reynolds number is not matched. For the smooth wall case Re_τ = 1400, whereas Re_τ reaches 1900 at the final station downstream of the R→S surface change.

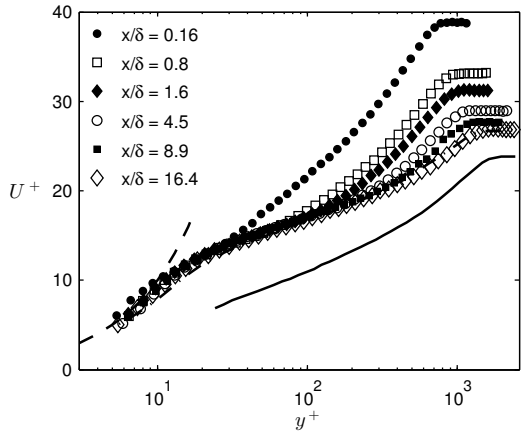

Figure 4. Inner viscous scaling of selected mean streamwise velocity profiles. Symbols correspond with figure 3.

Turbulence statistics of the streamwise velocity are calculated from the single hot-wire signal and are shown in

figure 5 and figure 6 for the outer and inner normalization, respectively. Successive profiles of $\overline{uu}/U_\infty^2$ exhibit two distinct energetic regions over the smooth wall following the R→S surface change. Comparing these profiles with that nearest the rough surface shows that the hump occurring in the region $y/\delta > 0.05$ is an artifact of the turbulence produced over the rough-wall. This is consistent with rough wall boundary layers as discussed by Jiménez (2004) where a peak occurs in the logarithmic region, often between $y/\delta = 0.05 - 0.2$. This hump both decreases in magnitude and moves away from the wall with fetch from the R→S interface. The rate that the hump migrates away from the wall is clarified by considering the location of the internal boundary layer.

The internal layer represents the mean extent to which the different boundary conditions have influenced the flow. Methods to locate the internal boundary layer are proposed by Andreopoulos & Wood (1982) and Antonia & Luxton (1972). The former employs streamwise differentiation of successive mean velocity profiles, whereas the latter relies on the dependence of the velocity gradient on the local wall shear stress. Due to the limited streamwise locations considered, the latter method is utilized. The edge of the internal layer was determined from the inflection of the mean velocity profiles plotted in the form $U/U_\infty \propto y^{1/2}$. The internal layer growth rate was captured by the well by $\delta_i/\delta = 0.12(x/\delta)^{0.43}$. As shown in figure 5 and figure 6, the outer region peak turbulence resides above this layer and tracks with this location downstream.

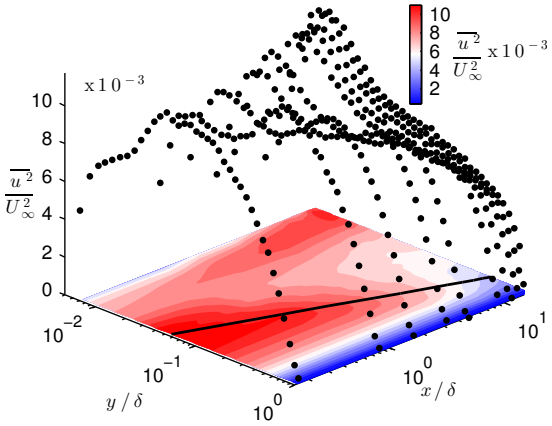

Figure 5. Outer scaled profiles of $\overline{u^2}$ and resulting contour map, the internal boundary layer is shown by ——. Data markers show all measurement locations up to δ.

Within the internal boundary layer it is evident from the outer scaling of $\overline{u^2}$ that an additional peak develops over the smooth surface, due to the near wall cycle, as shown in figure 5. This peak appears immediately. For the profile nearest the R→S interface it manifests as a kink in the wall-normal profile. The peak continues to develop and grows in strength while migrating nearer the wall as is evident from the contours shown in figure 5 for $y/\delta < 0.05$. By scaling the streamwise stress with the local friction velocity, $\overline{u^2}/U_\tau^2$, the inner peak location collapsed, as shown in figure 6, at approximately $y^+ = 14$, which is consistent with comparable smooth wall observations. For both the inner and outer

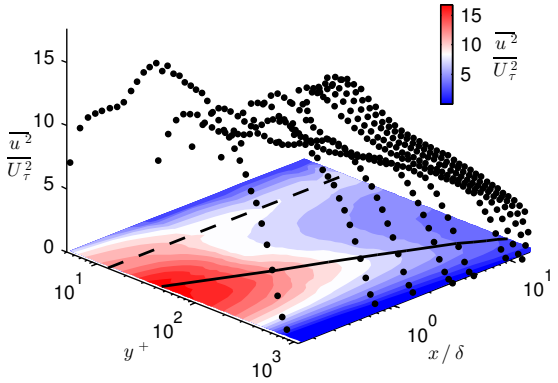

Figure 6. Inner scaled profiles of $\overline{u^2}$ and resulting contour map, the internal boundary layer is shown by —— and y^+ = 14 is indicated by – – –.

energetic regions, the peak streamwise stress decreased in magnitude under inner scaling with the downstream location. However, for smooth flat plate turbulent boundary layers in equilibrium the peak value of $\overline{u^2}/U_\tau^2$ is known to increase with Re_τ. Hutchins & Marusic (2007*a*) described the increase in the peak inner value by $(\overline{u^2}/U_\tau^2)_{peak} = 1.036 + 0.965\ln(\mathrm{Re}_\tau)$. Past the R→S change in surface roughness both the shear stress and boundary layer thickness increased, which implies an increase in Re_τ. However, the inner variable scaled streamwise stress decreased immediately following the R→S interface, as is shown in figure 6. Past approximately $x/\delta > 12$ the magnitude of the near wall peak reached the empirical value of $(\overline{u^2}/U_\tau^2)_{peak}$ given by Hutchins & Marusic (2007*a*), which is consistent with a near equilibrium condition as shown in figure 1.

Since the statistics of the streamwise velocity fluctuations represent the combined influence over all scales, the temporal spectra of the streamwise fluctuations, ϕ_{uu}, is examined to investigate how the near-wall and outer regions of the boundary layer manifest energetically following the R→S surface change. The local convective velocity is used to express the temporal spectra as a function of streamwise wavenumber, $k_x = 2\pi U$, and wavelength, $\lambda_x = 2\pi/k_x$. Spectra are pre-multiplied by the wavenumber, k_x, and normalized by the local friction velocity, *viz.* $k_x\phi_{uu}/U_\tau^2$. Contours of the pre-multiplied spectra are assembled from the data at each wall-normal location, which gives a physical sense of the distribution of the energetic composition across the boundary layer, as is shown in figure 7. The spectra contours downstream of the rough to smooth surface change (see figure 7) exhibit a distinct bimodal appearance. The location of the inner peak of $\overline{uu}/U_\tau^2$ determined from figure 6 at $y^+ \approx 14$ is indicated at $\lambda_x \approx 1000$ in figure 7 at the approximate location of the local inner peak of $k_x\phi_{uu}/U_\tau^2$. Above the near-wall region an outer region peak in $\overline{u^2}/U_\tau^2$ is observed in figure 5 and as shown in figure 7 the turbulent motions are of a wavelength centred about $\lambda_x \approx 3\delta$, which represents large scale motions, see for example Monty *et al.* (2009). Also, as noted by Hutchins & Marusic (2007*b*) a peak in the boundary layer spectra map occurs at $y/\delta \approx 0.06$, corresponding to superstructures of wavelength $\lambda_x \approx 6\delta$ for higher higher Reynolds numbers. The signature of these structures is only marginally visible in the spectra contours shown here. It is also evident that the peak energy in the near-wall region decreased again down-

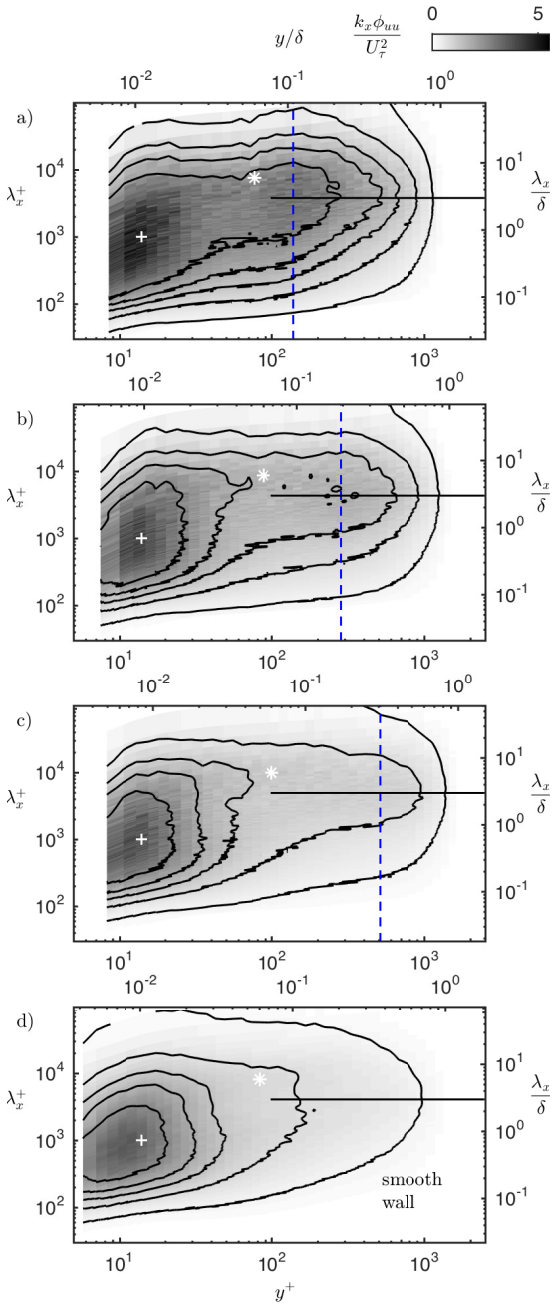

Figure 7. Pre-multiplied spectrum, $k_x\phi_{uu}/U_\tau^2$, following the rough to smooth change in surface. The location of the approximate peak in $\overline{u^2}$ is indicated at $y^+ = 14$ and $\lambda_x^+ = 1000$. The location of the internal boundary layer is identified by – – –. a) $x/\delta = 0.8$ b) $x/\delta = 3.1$ c) $x/\delta = 8.9$ d) smooth wall case.

stream, albeit slowly compared to the decrease occurring in the outer region following the R→S surface change.

The structure of the boundary layer is considered by the two-point spatial correlation of the PIV vector fields about a reference (x_{ref}, y_{ref}) location, *viz.*

$$R_{uu}\left(x_{ref},y_{ref},x,y\right) = \frac{\overline{u\left(x_{ref},y_{ref}\right)u\left(x,y\right)}}{\sigma_u\left(x_{ref},y_{ref}\right)\sigma_u\left(x,y\right)}, \qquad (1)$$

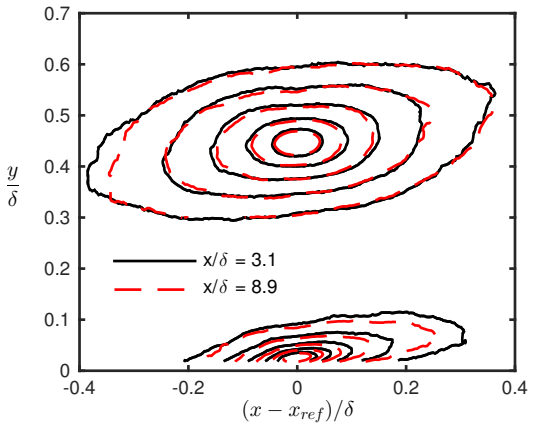

Figure 8. Contours of R_{uu} with x_{ref} and y_{ref} at $x/\delta = 3.1$ and 8.9 and $y/\delta = 0.45$ and 0.025. Contour levels are at 0.5, 0.6, 0.7, 0.8, and 0.9.

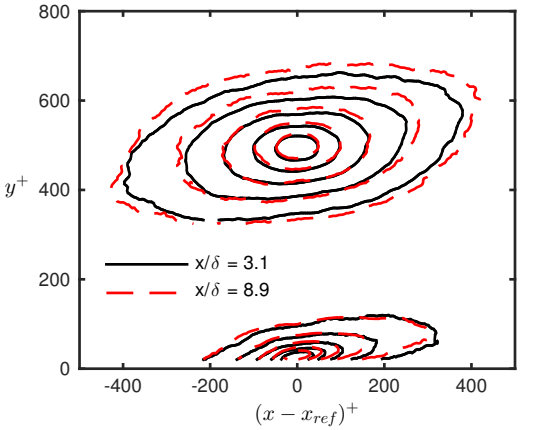

Figure 9. Contours of R_{uu} with x_{ref} and y_{ref} at $x/\delta = 3.1$ and 8.9 and $y^+ = 500$ and 32. Contour levels are at 0.5, 0.6, 0.7, 0.8, and 0.9.

where the over-line represents the ensemble average of the 5000 vector fields. Figure 8 shows contours of the correlation, R_{uu}, centred about two wall-normal locations, $y/\delta = 0.45$ and 0.025, at two downstream locations, $x/\delta = 3.1$ and 8.9. Note that the lower wall-normal value is limited by reliable vectors, for which the first two nearest the wall were discarded. The structure of the outer region appears to be similar at each downstream location, whereas the contours of the near-wall flow are different. The structure appears similar for inner unit scaling in the near-wall region, as is shown in figure 9 at $y^+ = 32$, whereas the contours then fail to collapse at $y^+ = 500$. This suggests that the outer region may be independent of the near-wall condition whereas the near-wall flow may depend on the outer-flow behaviour. Moreover, the structure inclination appears consistent following the R→S change in surface as is clear from these figures, which agrees with observations of independently rough- and smooth-wall boundary layers as shown by Volino *et al.* (2007), for example.

CONCLUSIONS

Experimental measurements of a boundary layer over a surface that changes from a rough to smooth wall condition were made. The flow field was interrogated by hot-wire anemometry and particle imaging velocimetry while the local skin friction is determined by Preston tube measurements. An internal boundary layer represents the demarkation between the characteristic flow of the upstream rough wall condition and the region developing over the smooth surface. The inner and outer regions of the flow can be described in terms of inner and outer variables. The outer turbulence peak tracked the development of the internal boundary layer and decayed downstream such that the initial bimodal appearance of the spectral energy distribution diminished. In contrast, within the internal layer the location of the inner peak collapsed by the inner viscous scaling. However, the magnitude of this peak does not scale according to the equilibrium smooth. The near wall peak appears overly energetic due to the turbulence remaining in the outer region from the upstream condition. In addition, the structure of the outer region appears collapse based only on the outer length scale, δ, and appeared to be independent of the near-wall condition, which was consistent with recent results of comparable rough and smooth wall flows. However, the structure of the near-wall region does not collapse accordingly with the outer scaling, it depends on the local near-wall condition.

REFERENCES

Andreopoulos, J. & Wood, D. H. 1982 The response of a turbulent boundary layer to a short length of surface roughness. *Journal of Fluid Mechanics* **118**, 143–164.

Antonia, R. A. & Luxton, R. E. 1972 The response of a turbulent boundary layer to a step change in surface roughness. part 2. rough to smooth. *Journal of Fluid Mechanics* **53**, 737–757.

Birch, D. M. & Morrison, J. F. 2011 Similarity of the streamwise velocity component in very-rough-wall channel flows. *Journal of Fluid Mechanics* **668**, 174–201.

Bruun, H. H. 1995 *Hot wire anemometry: principles and signal analysis*. Oxford University Press.

Burattini, P. & Antonia, R. A. 2005 The effect of different x-wire calibration schemes on some turbulence statistics. *Experiments in Fluids* **38**, 80–89.

Flack, K. A., Schultz, M. P. & Shapiro, T. A. 2005 Experimental support for townsend's reynolds number similarity hypothesis on rough walls. *Physics of Fluids* **17** (3), 035102.

Hutchins, N. & Marusic, I. 2007*a* Evidence of very long meandering features in the logarithmic region of turbulent boundary layers. *Journal of Fluid Mechanics* **579**, 1–28.

Hutchins, N. & Marusic, I. 2007*b* Large-scale influences in near-wall turbulence. *Royal Society of London Philosophical Transactions Series A* **365**, 647–664.

Hutchins, N., Nickels, T. B., Marusic, I. & Chong, M. S. 2009 Hot-wire spatial resolution issues in wall-bounded turbulence. *Journal of Fluid Mechanics* **635**, 103.

Jiménez, J. 2004 Turbulent Flows Over Rough Walls. *Annual Review of Fluid Mechanics* **36**, 173–196.

Loureiro, J. B. R., Sousa, F. B. C. C., Zotin, J. L. Z. & Silva Freire, A. P. 2010 The distribution of wall shear stress downstream of a change in roughness. *International Journal of Heat and Fluid Flow* **31** (5), 785 – 793.

Monty, J. P., Hutchins, N., Ng, H. C. H., Marusic, I. & Chong, M. S. 2009 A comparison of turbulent pipe, channel and boundary layer flows. *Journal of Fluid Mechanics* **632**, 431–442.

Nagib, H. M., Chauhan, K. A. & Monkewitz, P. A. 2007 Approach to an asymptotic state for zero pressure gradient turbulent boundary layers. *Royal Society of London Philosophical Transactions Series A* **365**, 755–770.

Österlund, J. M., Johansson, A. V., Nagib, H. M. & Hites, M. H. 2000 A note on the overlap region in turbulent boundary layers. *Physics of Fluids* **12**, 1–4.

Smits, A. J. & Wood, D. H. 1985 The response of turbulent boundary layers to sudden perturbations. *Annual Review of Fluid Mechanics* **17**, 321–358.

Taylor, R. P., Taylor, J. K. & Coleman, H. W. 1993 Relation of the turbulent boundary layer after an abrupt change from rough to smooth wall (data bank contribution). *Journal of Fluids Engineering* **115** (3), 379–382.

Volino, R. J., Schultz, M. P. & Flack, K. A. 2007 Turbulence structure in rough- and smooth-wall boundary layers. *Journal of Fluid Mechanics* **592**, 263–293.